

Article

# Fatigue Cycles and Performance Evaluation of Accelerating Aging Heat Treated Aluminum Semi Solid Materials Designed for Automotive Dynamic Components

Mohamed Attia <sup>1</sup>, Khaled Ahmed Ragab <sup>1,2,\*</sup>, Mohamed Bouazara <sup>1</sup> and X.-Grant Chen <sup>1</sup>

<sup>1</sup> Department of Applied Sciences, University of Quebec, Chicoutimi, QC G7H2B1, Canada; mohamed.attia1@uqac.ca (M.A.); mbouazar@uqac.ca (M.B.); xgrant\_chen@uqac.ca (X.-G.C.)

<sup>2</sup> Department of Metallurgy, Faculty of Engineering, Cairo University, Giza 12613, Egypt

\* Correspondence: khaled.ragab@uqac.ca; Tel.: +1-(418)-545-5011 (ext. 2501)

Received: 5 April 2020; Accepted: 21 April 2020; Published: 26 April 2020



**Abstract:** The A357-type (Al-Si-Mg) aluminum semi solid casting materials are known for their excellent strength and good ductility, which make them materials of choice, preferable in the manufacturing of automotive dynamic mechanical components. Semi-solid casting is considered as an effective technique for the manufacturing of automotive mechanical dynamic components of superior quality performance and efficiency. The lower control arm in an automotive suspension system is the significant mechanical dynamic component responsible for linking the wheels of the vehicle to the chassis. A new trend is to manufacture this part from A357 aluminum alloy due to its lightweight, high specific strength, and better corrosion resistance than steel. This study proposes different designs of a suspension control arm developed, concerning its strength to weight ratio. Furthermore, this study aims to investigate the effect of accelerating thermal aging treatments on the fatigue life of bending fatigue specimens manufactured from alloy A357 using the Rheocasting semi-solid technology. The results revealed that the multiple aging cycles, of WC3, indicated superior fatigue life compared to standard thermal aging cycles. On the other hand, the proposed designs of automotive suspension control components showed higher strength-to-weight ratios, better stress distribution, and lower Von-Mises stresses compared to conventional designs.

**Keywords:** low/high fatigue cycles; aluminum semi-solid; design analysis; finite elements

## 1. Introduction

A357-type aluminum (Al-Si-Mg) alloy is mostly known for its excellent strength and quality index value, and is widely used in various engineering applications, particularly in the automotive industry [1–4]. The vehicle suspension system is the assembly of mechanical components located between the frame (chassis) of the vehicle and road wheels. The suspension system is responsible of absorbing shocks from the road, maintaining contact between vehicle tires and the road, transmitting applied power from vehicle wheels to the chassis, and maintaining the proper kinematics of suspension. The suspension system usually consists of three main components: springs, dampers, and suspension linkage. Springs and dampers are responsible for the response of the vehicle under random excitations from different road conditions (and they are the subjects of research in many automotive vibration studies), while suspension linkages are the assemblies of mechanical components, linking the whole suspension system and transmitting forces to the chassis of the vehicle [5,6]. Manufacturing this mechanical component from light metals helps with enhancing vehicle performance by decreasing the unsprung mass. Several studies indicate superior mechanical performance by using semi-solid

casting technology for producing such automotive suspension mechanical components of aluminum alloy [1,5–7].

Semi-solid forming (SSF) is a forming technique that combines the processes of casting, forming, and extrusion. Force is applied, either mechanical or electromagnetic, to fragment the semi-solid structure in the mushy zone of liquid–solid range. Temperature is retained above melting point for the whole process. It is then compressed inside the mold cavity under high pressure to take its final geometry [8,9]. Semi-solid is classified into two casting techniques: thixocasting and rheocasting. Thixocasting involves the formation of the required billets with desired microstructure from continuous casting, which is obtained, usually, by electromagnetic stirring. While in rheocasting, liquid metal is poured in an equal size container with the die to be filled, and is then fed to the die chamber; this avoids the reheating process of stock metal. The semi-solid materials (SSM) mix is produced and injected on demand, which decreases the total cycle time and, thus, cost. The desired structure is obtained by cooling, grain refinement, and stirring. The semi-solid casting process is characterized by the presence of equiaxed grain structure compared to the dendritic structure found in conventional casting [8–12].

In addition to the positive effects of using semi solid casting technique, the accelerating thermal aging treatments, using multiple and interrupted cycles, result in superior mechanical properties compared to traditional thermal treatments. A study done by Zhy et al. [13] showed the effect of multiple thermal aging over traditional single step aging for alloy A357. Samples were solution heat treated at 543 °C for 12 h then quenched in water maintained at 80 °C. Single stage aging was done at temperatures of 155, 165, and 175 °C for 4 h to 16 h. For step aging, samples were pre-aged at 155 °C for 4 h then finally aged at 175 °C for 3 h to 18 h. The results showed an enhancement in the strength and ductility values of samples that were step aged for 12 h. What was also observed were the general enhancements in the tensile properties of the step aged samples on the single aged samples. The explanation of the high strength and ductility was related to the presence of different precipitate sizes of Mg<sub>2</sub>Si. Other studies [14,15] applied TEM study on the effect of multiple thermal aging treatments on performance and precipitate evolution of A357 semi-solid samples. Moreover, the formation of different sizes of Mg<sub>2</sub>Si precipitates that compromise between excellent strength and high ductility was observed. The strengthened precipitates showed large differences in sizes as a result of the multiple thermal aging cycles [14]. Therefore, applying the multiple step thermal aging cycles to the aluminum semi-solid casting alloy in the manufacturing of the suspension control arm is expected to increase the total fatigue life of this component [15–17].

The main objectives of this study are to improve the fatigue life cycles of aluminum semi solid materials and to obtain high qualified automotive suspension mechanical components by means of metallurgical and design parameters. This study aimed to investigate the effect of accelerating thermal aging treatments using multiple and interrupted cycles on the fatigue cycles of A357 (Al-Si-Mg) aluminum semi solid alloys. The design modifications and stress analyses were applied in this work using modeling and finite element techniques.

## 2. Materials Processing and Design Procedures

The standard samples and the applicable parts were prepared by the rheocasting semi-solid process using A357 aluminum alloy billets (Al-7%Si-0.65%Mg-0.1%Fe) as applied in [14,15]. The semi solid casting process is coupled with a high pressure die casting (HPDC) press to produce the materials used for mechanical and micro-structural characterizations. Figure 1 shows the accelerating thermal aging treatments using multiple and interrupted cycles of T4/T6/T7. These thermal aging treatments were applied to the bending fatigue standard samples and to the applicable suspension mechanical components. Specific aging cycles, mainly T6, WA0, WA1, WB0, WC1, and WC3, were applied in this study according to their positive effects on both tensile and quality index characteristics by previous studies applied for A357 aluminum semi solid alloys [14,15]. The bending fatigue samples were subjected to two step solution heat treatments, followed by water quenching maintained at 60 °C and then naturally aged at room temperature for 24 h before proceeding to the thermal aging cycles.

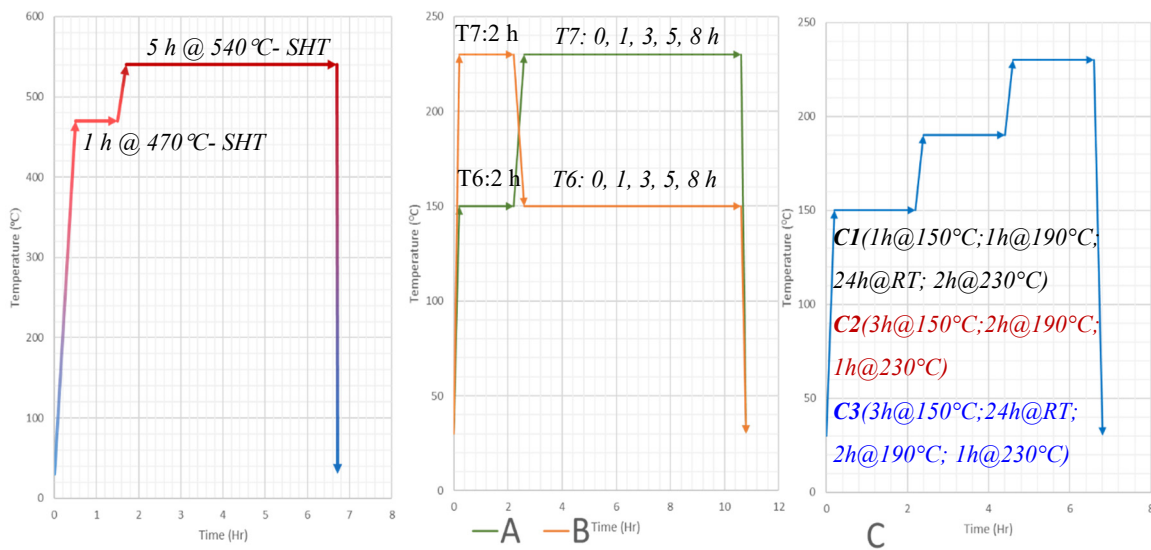


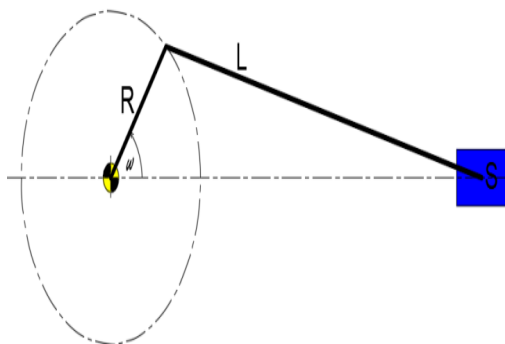
**Figure 1.** Accelerating thermal aging cycles; (A) T6/T7 aging, (B) T7/T6 aging, (C) multiple thermal aging cycles.

Fatigue cycles and performance were applied for both standard bending fatigue samples and applicable suspension control parts of A357 semi solid materials using bending high cyclic fatigue tests and tension-compression low cyclic fatigue, respectively. The constant deflection cantilever bending fatigue testing was applied in this study. Specimens were subjected to constant deflection for a high number of cycles until fracture. The bending fatigue samples were mounted, to be completely restrained from one end, while the other end was attached to the machine rocker arm. The rocker arm was adjusted so that it maintained a constant stroke throughout the whole experiment regardless of the load on each specimen. The machine used was a crank-slider mechanism in which the specimen was attached to the slider part. Figure 2a shows a crank-slider mechanism representing the operating mechanism of the testing machine. The specimen was mounted in the slider position ‘S’ while the motor rotated the crank ‘R’ with a constant angular velocity ‘ $\omega$ ’. The stroke length is of importance in this machine as it represents the deflection to be applied on the specimen. The stroke length can be altered by changing the length of the crank ‘R’. The fatigue test machine used in this experiment uses an eccentric crank in which the eccentricity works as the crank length. Thus, changing the eccentricity of the device would change the stroke length and the deflection applied to the test specimen. Figure 2b shows the eccentric crank in which the stroke can be adjusted from 0 to 2.0 inches (50.8 mm). The machine used operates using an electric motor of 0.5 HP (373 Watt) power and a maximum force transmitted to specimens of 40 lb (178 N). Operating frequency was set to 12 Hz for all test samples with a deflection of 6.35 mm (0.25 in). The samples were machined as shown in Figure 2c, and were then grinded to remove any scratches resulting from machining. Scratches and macro cracks act as stress raisers initiating fatigue cracks and causing much lower fatigue life. A MATLAB code was used in the calculation of the stress developed in the fatigue specimen using Young’s modulus of 70 GPa for aluminum, and Poisson’s ratio of 0.33 for isotropic material. Solid mechanic equations were used in the stress calculation as follows:

$$I = (bh^3)/12 \ \& \ \sigma = my/I \tag{1}$$

where ‘I’ is the 2nd moment of area, ‘b’ is the specimen width, ‘h’ is the specimen thickness, ‘ $\sigma$ ’ is the stress, ‘m’ is the maximum bending moment, and ‘y’ is half the thickness. Figure 2d shows the resulting plot of the code, showing a maximum stress of 50 MPa at the center of the reduced width area; stress then decays, reaching zero near both the restrained and the free ends. Regarding the applicable suspension control components shown in Figure 3, fatigue low cyclic tests were performed using a servo-hydraulic machine in sinusoidal force control at room temperature under force-controlled

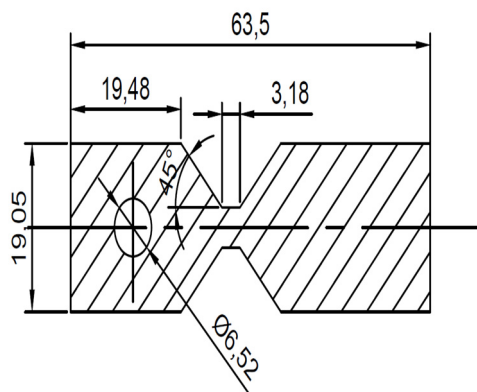
conditions at a frequency of 1 Hz. Sinusoidal forms of stress-compress loads varied from  $\pm 105$  MPa to  $\pm 280$  MPa, and were controlled by applying displacements varied from  $\pm 1$  to  $\pm 2$  mm.



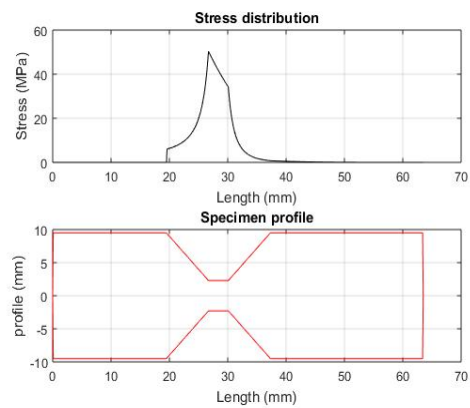
(a) Explanation of crank-slider mechanism of fatigue machine



(b) Constant deflection cantilever bending fatigue machine



(c) High cyclic fatigue specimen (Dimensions in mm)



(d) MATLAB stress distribution plot of cantilever bending specimen

**Figure 2.** Bending fatigue test using standard samples of A357 aluminum semi solid materials.

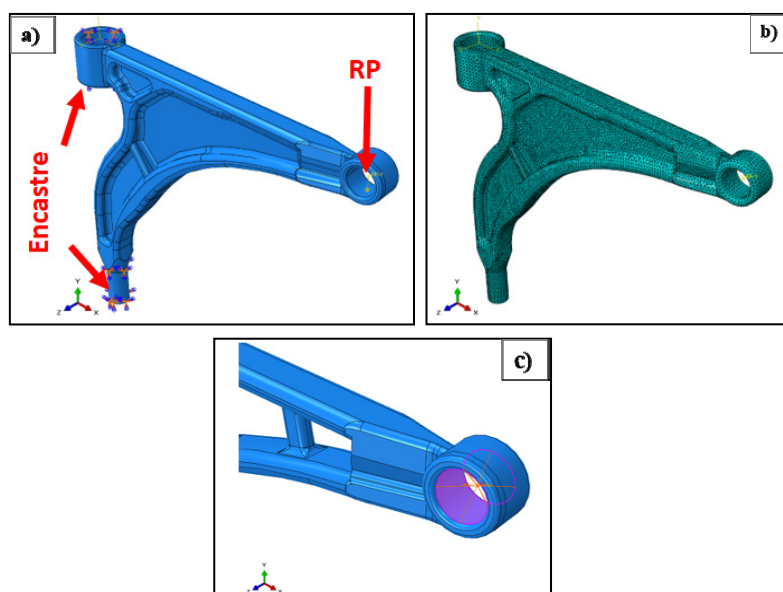


**Figure 3.** Finite elements configuration. (a) Boundary conditions, (b) meshing of the control arm part, and (c) multiple point constraint (MPC) interaction.

Regarding the design procedures, the design parameters of applicable parts had to consider the stress distribution, von Mises stress value, and strength-to-weight ratio. The design modifications and finite elements of suspension control arms were applied using computer-aided design (CAD) software SolidWorks 2018. The finite elements analysis (FEA) was performed using the Abaqus Complete Abaqus Environment (CAE) 2018 finite elements package. Figure 3 indicates the finite elements configuration of the applicable suspension control arm used in this study. The multiple point constraint (MPC) beam represents the most appropriate loading condition, to be most similar to real loading conditions. In order to do that, a complete understanding of the loads exerted on the suspension control arm is required. Forces acting on vehicle tires can be calculated in the three dimensions  $x$ ,  $y$ , and  $z$ ; such that the  $x$ -component is the longitudinal force ( $F_{Long}$ ), the  $y$ -component is the lateral force ( $F_{Lat}$ ), and the  $z$ -component is the vertical force ( $F_V$ ), as shown in Figure 4. While the vertical force is due to the vehicle weight, and the lateral force is due to camber and toe angles, the force of importance in this study is the longitudinal force. It is induced as a result of the rolling resistance force, as well as traction-compression cycles due to braking [18].

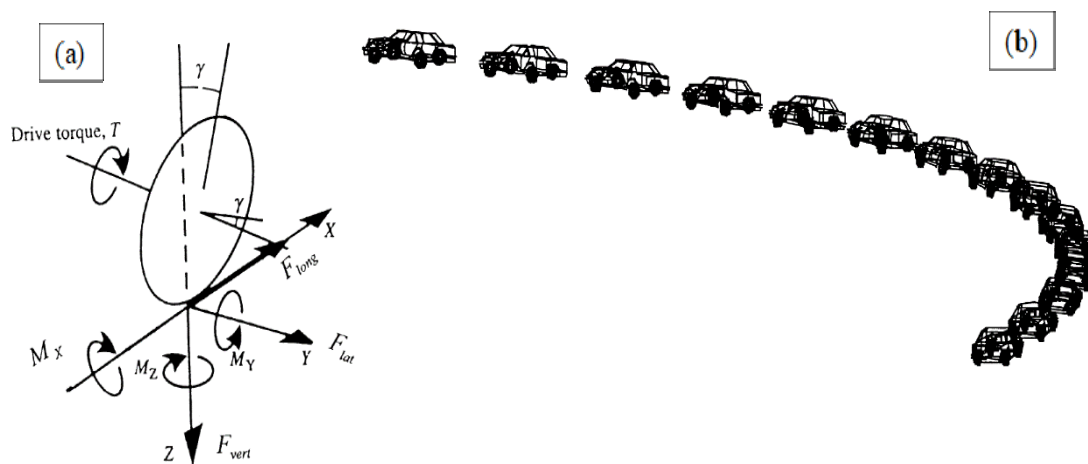


**Figure 4.** (a) Forces acting on vehicle tires due to engine torque, (b) simulated vehicle maneuver for 5s [18].

### 3. Results and Discussions

#### 3.1. Fatigue Cycles and Performance

The high cycle fatigue bending test and the low cycle fatigue compression-traction test were applied in this study on the standard bending fatigue samples and the automotive suspension control components of aluminum semi solid materials, respectively. Table 1 shows the low cyclic fatigue results of the control arm part heat treated using standard T6 and multiple thermal aging heat treatment cycles. Regarding the low cycle fatigue test, one applicable part was tested for each thermal aging condition. There was a slight increase in fatigue life for the thermal aging cycle of WA0 (40,000 cycles) compared to standard T6 (36,000 cycles); while significant enhancement for the thermal aging cycle of WC3 resulted in superior values (72,000 cycles). The other aging cycles did not show a notable enhancement of fatigue life over the standard T6. It is well known that the fatigue performance is highly affected by the strength and ductility properties of the aluminum matrix. A good combination of excellent strength and high ductility can postpone the fatigue cracking failure and increase the fatigue life—number of cycles [14–17]. For these reasons, the accelerating multiple thermal aging cycles of WC3 were applied to enhance the fatigue mechanical properties, by having compromised values of optimum strength and acceptable ductility compared to those obtained by standard thermal treatments.

**Table 1.** Fatigue cycles of the A357 aluminum semi-solid applicable parts.

Thermal Aging treatment	Fatigue Cycles
WA0 (T6/T7) Multiple thermal aging cycles	40,000 cycles
WA8 (T6/T7) Multiple thermal aging cycles	24,000 cycles
WB0 (T7/T6) Multiple thermal aging cycles	30,000 cycles
WC1 (T4/T6/T7) Multiple thermal aging cycles	33,000 cycles
WC3 (T4/T6/T7) Multiple thermal aging cycles	72,000 cycles
T6 Standard thermal aging	36,000 cycles

Regarding the bending fatigue test, the results of the experiment are plotted in the chart shown in Figure 5 and a moving average spine was fitted between the original test values. The results revealed a remarkable increase in the fatigue life of the WC3 thermal aging cycle compared to the standard T6 aging. The results went well, with both results of the applicable part fatigue testing, as well as the results of the tensile testing and quality index indicated in previous works [14,15]. The multiple thermal aging treatments of WA0 and WC1 show nearly similar average fatigue values of 54,667 and 53,000 cycles, respectively, compared to the standard T6 with 53,000 fatigue cycles. On the other hand, the thermal aging treatment WA1 (59,250 fatigue cycles) showed an enhancement of fatigue life compared to T6. The multiple thermal aging of WB0 showed lower fatigue cycles than T6 with only 25,000 cycles, indicating undesirable mechanical properties for all multiple thermal aging treatments of B cycles. A remarkable 155% enhancement of fatigue life for the interrupted thermal aging treatment of WC3, with an average of 82,000 cycles, which proves its significant impact for obtaining such superior fatigue cycles compared to standard thermal aging T6. This significant enhancement can be related to its high quality index values of excellent strength and high ductility. The WC3 interrupted thermal aging cycles, contributed in formation of well distributed and high density Mg<sub>2</sub>Si precipitates of various sizes, as explained in previous studies [14,15].

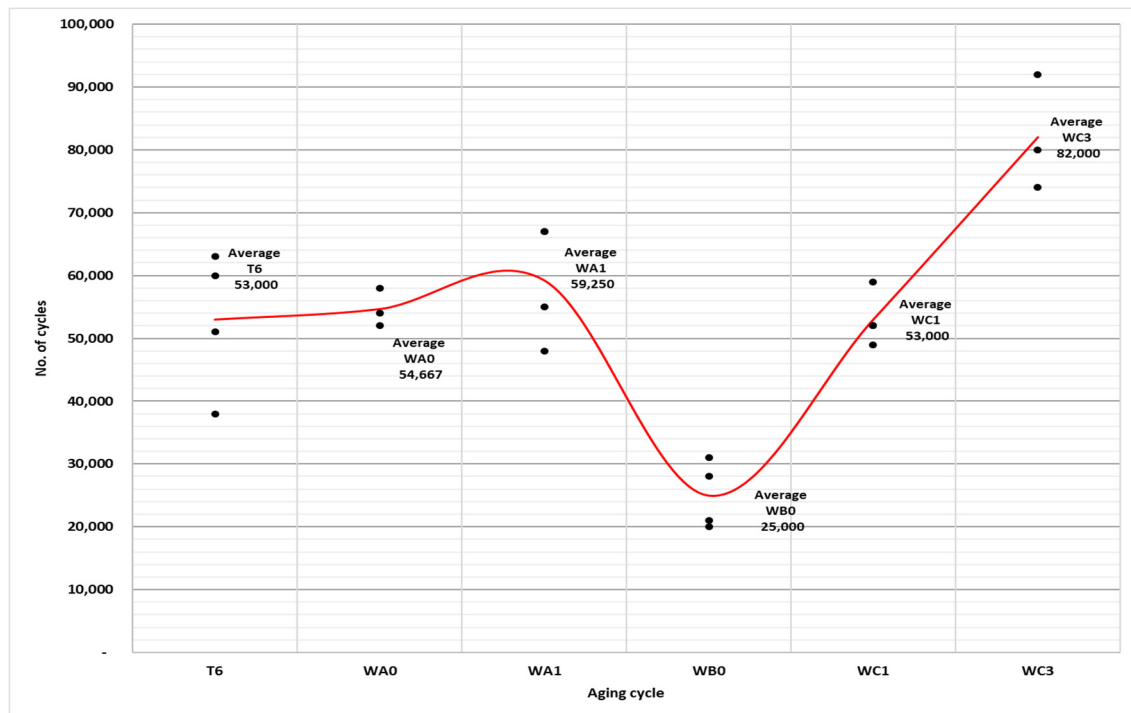


**Figure 5.** Results of cantilever bending fatigue test for standard samples.

### 3.2. Design Analysis and Finite Elements

The automotive suspension control arm components are subjected to loading forces applied in three directions as shown in Figure 4. Longitudinal force can be calculated by the combination of the rolling resistance force and the traction force. Rolling resistance force can be calculated by multiplying the coefficient of rolling friction ‘f’ with vehicle vertical load. While traction force can be calculated by multiplying the instantaneous value, the friction coefficient ‘μ’ with the vertical load. The equation can be written as follows:

$$F_{(long.)} = (\mu - f) * F_v \tag{2}$$

According to the understanding of applied forces on suspension mechanical structure, finite elements using Abaqus software was applied on the designs proposed in this study by SolidWorks software. Four designs were selected according to the applied forces, as well as specific design parameters that possessed excellent performance. Figure 6 shows the proposed designs in this study, which are mainly defined as follows: design 1 (inclined web with reinforcement ribs), design 2 (Planar thin web), design 3 (Hollow design) and design 4 (Trussed design).

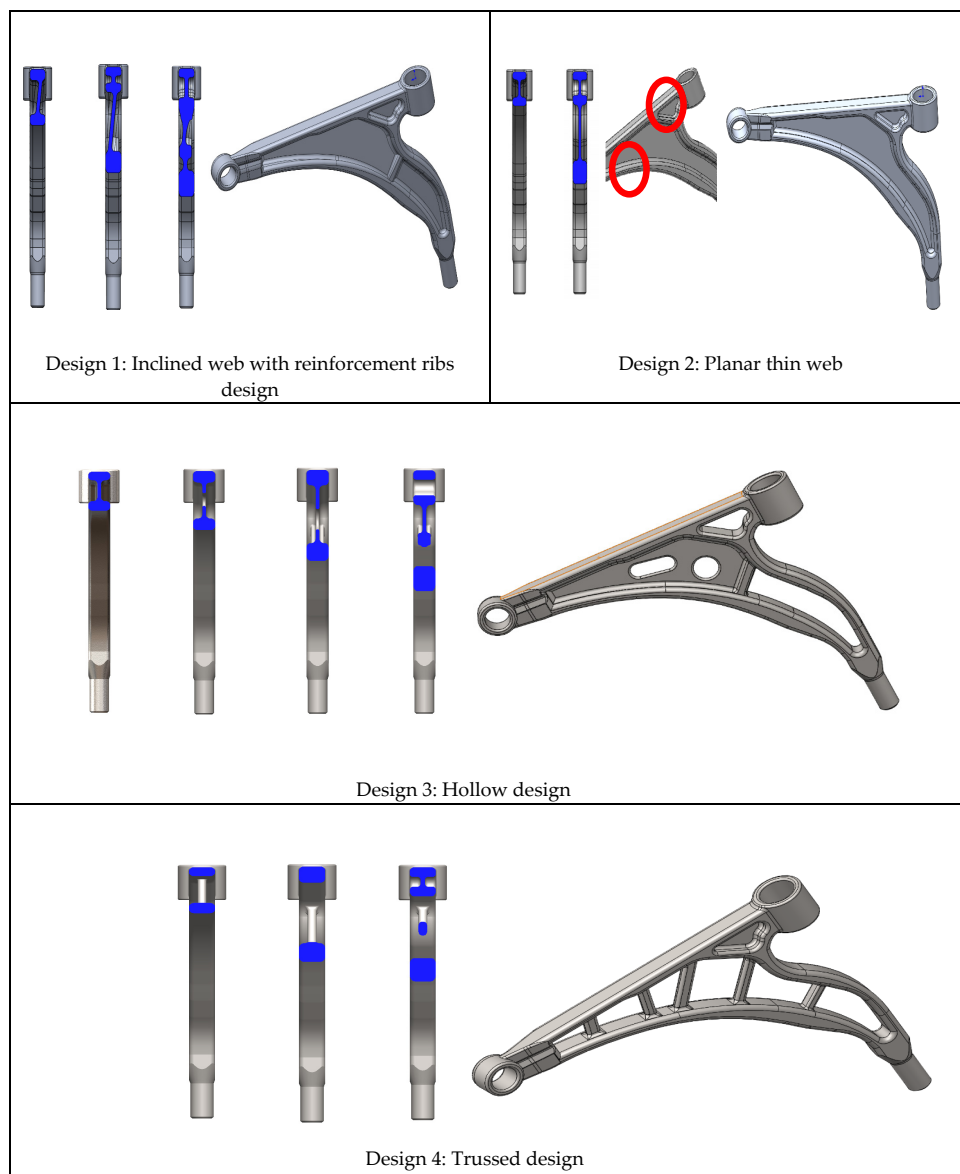


**Figure 6.** Modified design proposed for automotive mechanical suspension control arm structure.

The first design, inclined web with reinforcement ribs, followed the inclined Z-shaped web instead of the conventional straight design. Web inclination was set to  $7^\circ$ , relative to the normal of the plane parallel to the upper flange, as shown in Figure 6a, to compensate the  $5^\circ$  inclination of the ball socket. The angle of inclination was selected, after multiple trial and errors, using a different angle each time and carrying out FEA simulation. The structure was reinforced by means of a small rib at the lower part of the control arm to limit excess deformation under load. The total mass of the part was found to be 1198 g, which is nearly similar to that of the conventional design (1200 g). The result of the finite elements analysis of the inclined web design is shown in Figure 7. The maximum von Mises stress is found to be 213 MPa, observed near the lower bushing of the control arm. A maximum stress concentration factor (SCF) of 8 is observed near the lower bushing region. The maximum deformation at the location of the ball joint is 1.45 mm under the 5500 N force. A homogenous stress distribution in the lower flange is observed, as shown in Figure 7b, as a result of the inclined web that compensated the inclination of the ball joint socket. The inclination of the web instead of the ball socket leads to the presence of homogenous stress in the lower flange and the absence of any stress raiser regions.

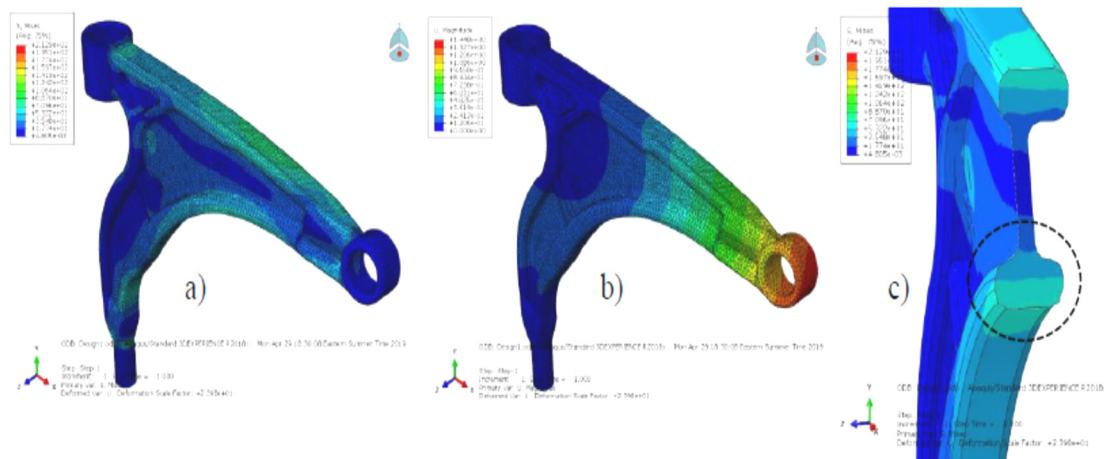


**Figure 7.** Finite elements analysis (FEA) of inclined web design. (a) von Mises stress plot, (b) total displacement plot, (c) cross-sectional stress distribution.

The second design relating to thin web design is the most basic design in the critical thinking of manufacturing of the part (due to its simple design). The design eliminates the use of any reinforcement ribs and increases thickness of the upper and lower flanges in critical stress regions. The middle web has a thickness of 4 mm, as shown in Figure 6b, which decreases the total mass of the control arm to 1141 g (by 59 g less than the conventional design). The decrease of weight is not considered enough for performance improvement; thus, elimination of more material is required. The results of the planar thin web design, shown in Figure 8, shows a maximum von Mises stress of 199 MPa. A maximum SCF of 9.95 is also observed near the lower bushing of the control arm in the location of maximum stress. The planar thin web design has nearly similar maximum deformation to the first design of 1.46 mm. The stress distribution in the lower flange is not homogeneous as the previous design due to the straight middle web. A SCF of 3.725 is also observed at the location of the arrow shown in Figure 8c. The design is observed to have high SCF values, despite the lower maximum von Mises stress.

The third proposed hollow design, shown in Figure 6c, is the evolution of the previous design with the removal of materials (where zero or little stress). One rib was added to the lower part of the control arm to increase the rigidity of the control arm in this critical region. The total mass of the structure was decreased to 1082 g; however, stress concentration regions are expected to occur near the hollowed regions, which may cause easier fracture. The formation of these stress concentration regions is due to the presence of holes in the web of the control arm. Therefore, a renovation of this design was needed that has the advantage of weight reduction without the use of pierced web. The solution of this

problem was found by the development of the succeeding design. The finite elements analysis (FEA) of the hollow design results are found in Figure 9. A maximum von Mises stress of 287 MPa is observed above the location of the lower bushing, higher than the two previous designs. The maximum SCF decreased significantly to 5.2 despite the very high stress. The maximum deformation is observed to be 1.69 mm, which is higher than all other previous designs. The high deformation and low SCF signifies that the stress is more homogenously distributed on the whole part. High stresses are observed near the locations of the holes marked with red arrows.

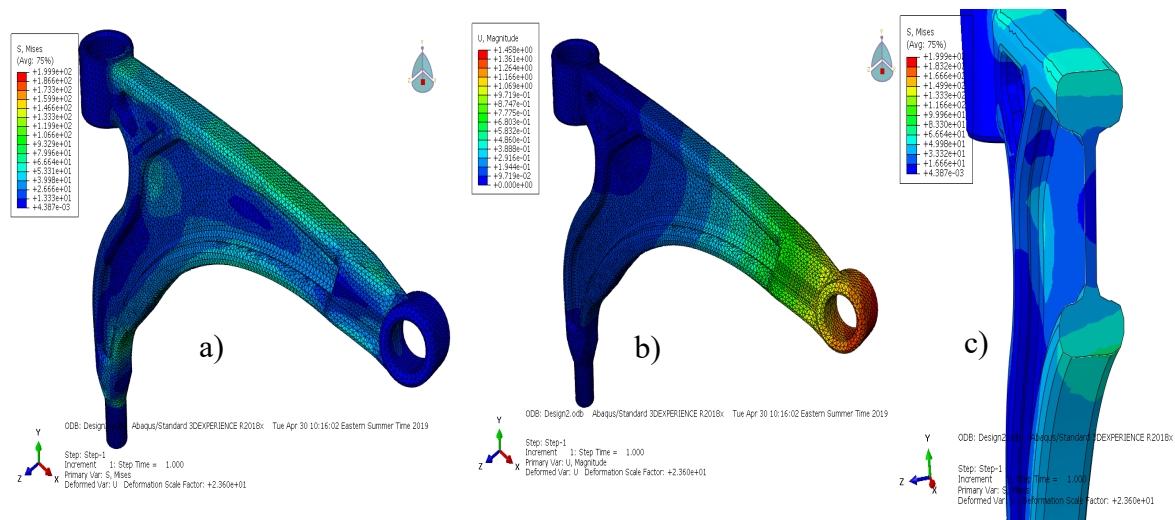


Figure 8. FEA of planar thin web design; (a) von Mises stress plot, (b) total displacement plot, (c) cross-sectional stress distribution.

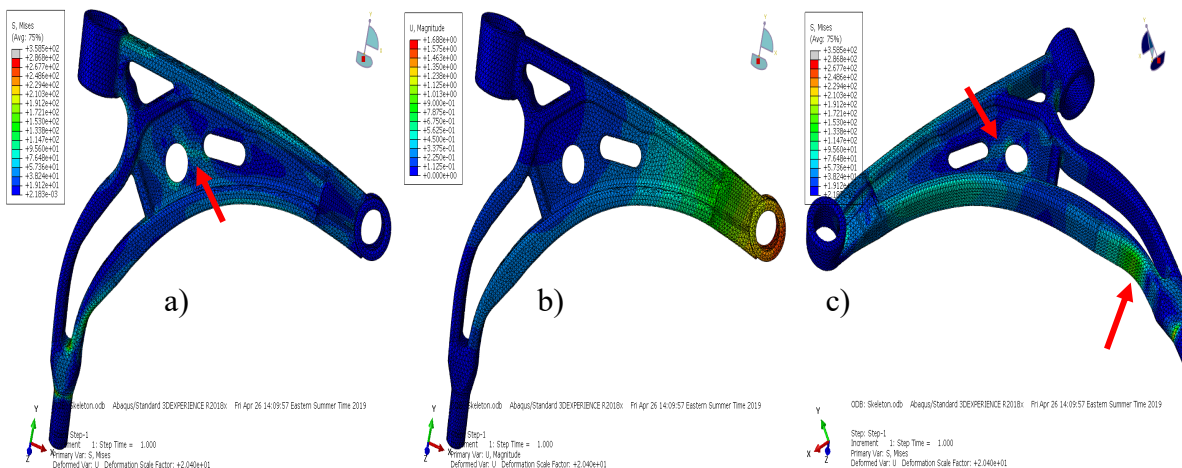


Figure 9. FEA of hollow design; (a) von Mises stress plot, (b) total displacement plot, (c) other view of Von Mises (VM) stress plot.

The trussed design was developed to solve the issue of stress concentration due to web piercing; thus, this design replaced the middle web with a number of ribs as shown in Figure 6d. Regarding this design, five ribs were developed to withstand the loading conditions and to connect the upper and lower flanges of the control arm. The idea of the design is to increase the flexibility of the control arm structure; thus, ensuring that the stress is distributed evenly throughout the whole part. The shape, number, dimensions, and locations of the ribs were selected, after multiple trial and errors, to compromise the weight and performance of the part. The trussed design is the lightest design, weighing only 1040 gm, making it the most efficient design in terms of weight. The design resembles

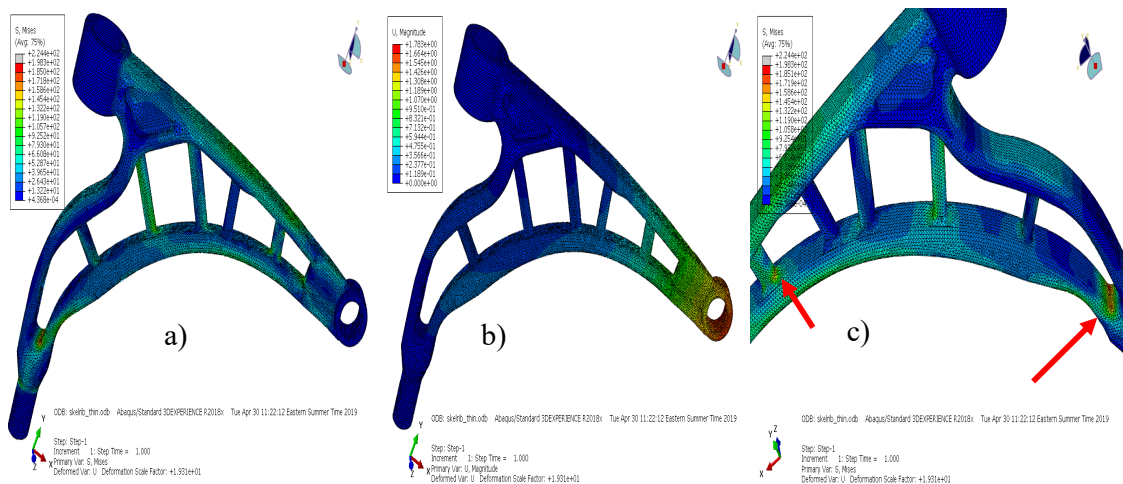
the shape of trusses found in many structures as bridges and steel buildings; hence, where its name comes from. The idea of the design is based on removing excess material and distributing loads on the whole structure of the control arm rather than the concentration of stress in particular regions and zero stress in others. The maximum von Mises stress of the trussed design is shown in Figure 10a is 198 MPa. A remarkable maximum SCF of 2.475 is observed, indicating a complete homogenous distribution of stress over the whole body of the control arm. A maximum displacement of 1.78 mm is found at the location of the ball joint. The maximum stress location is shifted from the previous designs and located near the location of the arrows. The design is less rigid than other designs and transfers the force evenly throughout the whole part.

Figure 11 shows a summary of the results of the four designs compared to the original design. The trussed design is observed to have the lowest maximum Von Mises (VM) stress and the lightest weight. Percentages of enhancement is calculated and colored for the ease of comparison between different designs. Percentages were calculated by using the relation as follows:

$$\text{Percentage of enhancement} = (\text{original value} - \text{new value}) / (\text{Original value}) \times 100$$

Another study applied by S. Hegazy et al. [18] created a model of a moving vehicle performing the maneuver shown in Figure 4b and calculating forces on wheel hub using automatic dynamic analysis of mechanical systems (ADAMS) software. The mass of the vehicle body used was 1185 kg and the results for the maximum longitudinal force were calculated to be around 1800 N. This value, multiplied by a suitable safety factor, can be used as a clear guide of the amount of force the control arm should be able to support. A simulation done by X. Ning et al [19] was done to optimize the ride comfort requirements using ADAMS software. The study used the values of 4–12.5 Hz as the most sensitive frequency range of the driver seat vertical axis weighting frequency, and a value of 0.5–2 Hz for horizontal frequency [19]. Another optimization study was carried out by Vigaruddin and Reddy [20], using Radioss software. The control arm used in that study was of the wishbone type. The three-dimensional (3D) model was created using the computer-aided design (CAD) software, CATIA V5. The part was meshed using HyperMesh, by using 10 node tetrahedral elements with topology optimization. Spider webs were used in each loading slot to better represent load action. The optimization tool solved for stress values, given the factors of safety and displacement as constraints. The objective function was to minimize the weight and material used of this part. The optimized design of the wishbone showed a 30% weight reduction than the original design. A number of ribs can be observed, which replaced the solid middle web of the original design. These ribs can give the structure its needed strength while minimizing the weight as much as possible.

Ragab et al [21] proposed three different designs of the lower control arm, seeking to enhance stress distribution and weight of this part. The Z-shaped design was recommended due to its good stress distribution as well as its superior castability compared to the conventional design. The inclined web in the Z-shaped design is believed to enhance stress distribution; thus, preventing stress raiser zones. The results of the von Mises stress distribution are shown in Figure 8, which shows a maximum value of 199 MPa when subjected to a 5.5 kN longitudinal force. What can also be observed is the high density of zero stress regions (blue regions), which indicate that this design is not optimum. Another study by Nadot et al. [22], applied on the lower control arm fabricated from nodular cast iron of 95% ferrite and 5% pearlite, was conducted to show the effect of casting defects, as well as loading cycles on the total fatigue life. Suspension arm samples were mounted in a fatigue machine and different loads were exerted to its end with a frequency of 10 Hz until failure. The study revealed that 90% of control arms have an infinite fatigue life at around 19 kN of maximum force for the cast iron suspension control arm. The study also concluded that the most common reason of fatigue failure results from oxides at the surface of the control arm.



**Figure 10.** FEA of trussed design; (a) von Mises stress plot, (b) total displacement plot, (c) other view of Von Mises (VM) stress plot.

Part Name	Conventional design	Inclined web w/ribs	Planar thin web	Hollow	Trussed
Mass (g)	1200 O.D.M	1198 99% of O.D.M*	1141 95% of O.D.M	1082 90% of O.D.M	1040 86% of O.D.M
Max. Von-Mises stress (MPa)*	232	213 8.2% ↑	199 14.2% ↑	287 -23.7% ↓	198 14.65% ↑
Max. displ. (mm)**	1.4	1.45	1.46	1.69	1.78

\* O.D.M = Original design mass.

\*\* Stresses and displacement were calculated at 5500 N of force applied on the center of ball joint hole.

**Figure 11.** Finite element (FEA) results obtained for the applicable parts with various designs proposed.

Regarding this research work, the application of WC3 multiple thermal aging treatments to the proposed trussed design may improve the fatigue performance to withstand more than 84,300 cycles, which is 134% enhancement of the part’s life. It can be calculated by extrapolating the values of stresses of the original and new design with the values of T6 compared to WC3.

### 3.3. Fracture Surface Analysis

Figure 12 shows the scanning electron micrographs, indicating the fracture surface of fatigue samples obtained from damaged parts of A357 aluminum semi solid materials. The fatigue failure is recognized by the metallographic appearance of the fracture surface, which starts with cracks initiation and is followed by its propagation. The fracture surface mainly shows two regions; a smooth region, which refers to brittle fracture by crack propagation, and a rough region, known by the presence of dimples, where the component indicates a ductile fracture manner. The crack initiation sites are

related to slip bands found in the alpha aluminum phase, as shown in Figure 12 for WC3 samples. Slip bands are regions where there is intense deformation due to the shear motion between crystal planes. The existence of slip bands in a local region leads to severe roughening of the surface; it leads to localization of plastic strain versus fatigue failure [1,9,23].

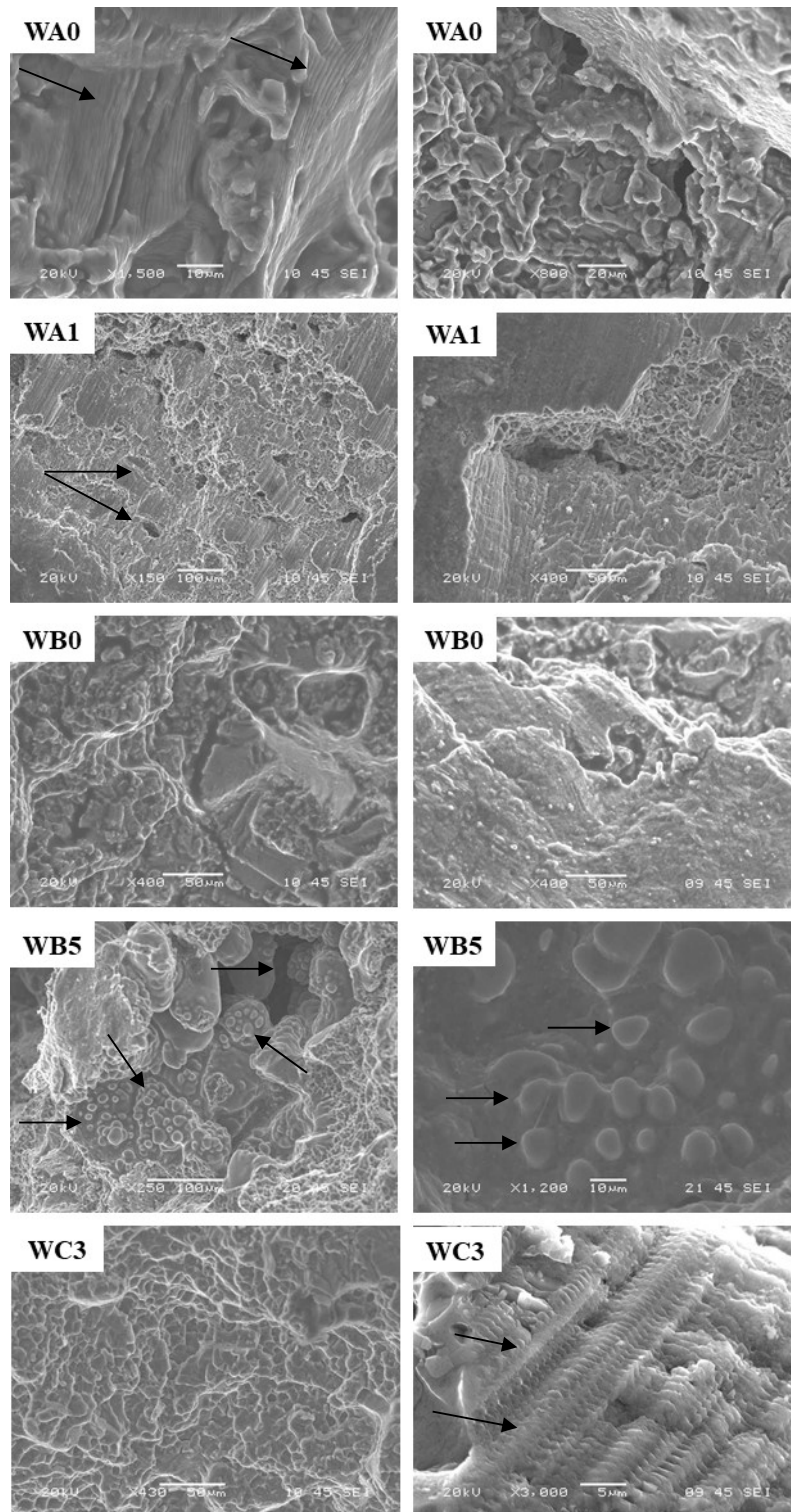


**Figure 12.** SEM micrographs of fracture surfaces due to fatigue failure of A357 aluminum semi solid samples heat treated by multiple thermal aging cycles.

The figure indicates the type of fracture, either ductile or brittle, for various thermal aging cycles investigated. For samples of WA0 and WC3, slip bands and beach marks were observed, indicating a complete fatigue failure and the absence of defects. In addition, the presence of dimpled structure, mostly for WC3 samples, indicates a ductile failure due to fatigue. A nearly defect-free microstructure for WC3, with the presence of slip bands and dimpled structure causing a ductile fatigue failure, can explain the high number of fatigue cycles for this thermal aging condition [1,23]. Porosities, referred by arrows, were observed for the WA1 and WB5 samples; hence, it was rejected due to its very low fatigue life cycles. In addition, the WB5 showed the presence of oxides, referred by arrows, in aluminum matrix, which had negative effects on the microstructure characteristics and fatigue performance of alloys investigated. These defects may highlight the problems and difficulties related to the semi-solid casting technique, which requires high precision and sophisticated equipment. For the control arm sample of WB0, the observed microstructure indicates a fatigue failure with a brittle structure. This brittle microstructure indicates an inductile material; hence, the crack propagation was very fast, that slip bands, referred by arrows, could not be clearly observed as those in WA0 and WC3 samples.

#### 4. Conclusions

Concerning to the fatigue cycles and design analysis of accelerating thermal aging treated A357 aluminum semi solid materials for the automotive suspension control components, the following conclusions can be drawn:

1. The multiple accelerating thermal aging cycles of WC3 shows a superior enhancement of real part fatigue life than the standard T6 with 72,000 cycles for C3, compared to 36,000 cycles for T6. The thermal aging cycles of WA0 also shows enhanced low cyclic fatigue life of 40,000 cycles and is considered more economical than T6.
2. The cantilever bending fatigue test reveals superior life cycles by applying the accelerating thermal aging treatment of WC3 with an average value of 82,000 cycles, compared to an average of 53,000 for T6. This proves the positive effect of multiple thermal aging treatments of WC3 on fatigue life. The aging cycle WA1 also shows enhancement over T6 with an average of 59,250 cycles; it is also considered more economical than T6.
3. The trussed design (design 4) of the applicable component shows superior properties than all other proposed designs in this paper—with a 160 gm lighter than the original design and a maximum VM stress of 198 MPa compared to 232 MPa for the original design. Design 4 is also more flexible than the original design, which can improve damping and increase the life of the ball joint connected to the control arm significantly. This flexibility is believed to better cushion road impacts resulting in better suspension behavior and comfort.
4. The application of selected WC3 multiple thermal aging treatments to the proposed design 4 (trussed design) is expected to withstand more than 84,300 cycles, which is 134% enhancement of the applicable part's life. This is calculated by extrapolating the values of stresses of the original and new design with the values of T6, compared to WC3.

**Author Contributions:** K.A.R., M.B., and X.-G.C. conceived and designed the experiments; M.A. and K.A.R. performed the experiments; M.A. and K.A.R. analyzed the data; M.A. applied design and finite elements analysis; M.A. and K.A.R. wrote the paper; K.A.R., M.B., and X.-G.C. revised the manuscript. All authors have read and agreed to the published version of the manuscript.

**Funding:** This research received no external funding.

**Acknowledgments:** Financial and in-kind support received from the CTA Aluminum Research Center, Chicoutimi, QC and the REGAL Aluminum Research Group of Laval University through the CURAL lab-University Research Center of Aluminum at the University of Quebec at Chicoutimi (UQAC), is hereby gratefully acknowledged.

**Conflicts of Interest:** The authors declare no conflict of interest.

## References

1. Bouazara, M.; Bouaicha, A.; Ragab, K.A. Fatigue characteristics and quality index of A357 type semi-solid aluminum castings used for automotive application. *J. Mater. Eng. Perform.* **2015**, *24*, 3084–3092. [[CrossRef](#)]
2. Rosso, M. The influence of casting process on quality and performances on Al based automotive components. In Proceedings of the 13th International scientific conference on Achievements in mechanical and materials engineering, Gliwice–Wista, Poland, 16–19 May 2005; pp. 547–550.
3. Fridlyander, I.N.; Sister, V.G.; Grushko, O.E.; Berstenev, V.V.; Sheveleva, L.M.; Ivanova, L.A. Aluminum alloys: Promising materials in the automotive industry. *Met. Sci. Heat Treat.* **2002**, *44*, 365–370. [[CrossRef](#)]
4. St John, D.; Caceres, C.; Zhang, D.; Edwards, G.; Taylor, J.; Schaffer, G. Aluminum alloys for cast automotive components. In Proceedings of the 2nd Conference and Exhibition on Materials in the Automotive Industry, IMMA, Melbourne, Victoria, Australia, 10–11 April 1996; pp. 140–143.
5. Bouazara, M.; Banitalebi, H.; Ragab, K.A.; Mrad, H. On the characteristics of automotive low arm-suspension system parts made of aluminum casting alloys. *Int. J. Cast Met. Res.* **2016**, *29*, 129–136. [[CrossRef](#)]
6. Bouazara, M.; Saoudi, A. Dynamic and Fatigue Study of the Automotive Upper Arm Suspension System. In *Advanced Materials Research*; Trans Tech Publications Ltd.: Stafa-Zurich, Switzerland, 2014; Volume 875, pp. 2269–2274.
7. Uys, P.E.; Els, P.S.; Thoresson, M. Suspension settings for optimal ride comfort of off-road vehicles travelling on roads with different roughness and speeds. *J. Terramech.* **2007**, *44*, 163–175. [[CrossRef](#)]
8. Doutre, D.; Langlais, J.; Roy, S. The seed process for semi-solid forming. In Proceedings of the 8th international conference on semi-solid processing of alloys and composites, Limassol, Cyprus, 21–23 September 2004; pp. 739–750.
9. Ragab, K.A.; Bouazara, M.; Bouaicha, A.; Allaoui, O. Microstructural and mechanical features of aluminium semi-solid alloys made by rheocasting technique. *Mater. Sci. Technol.* **2017**, *33*, 646–655. [[CrossRef](#)]
10. Langlais, J.; Lemieux, A. The SEED technology for semi-solid processing of aluminum alloys: A metallurgical and process overview. *Solid State Phenom.* **2006**, *116*, 472–477. [[CrossRef](#)]
11. Birol, Y. A357 thixoforming feedstock produced by cooling slope casting. *J. Mater. Process. Technol.* **2007**, *186*, 94–101. [[CrossRef](#)]
12. Flemings, M.C. Semi-solid forming: The process and the path forward. *Metall. Sci. Technol.* **2000**, *18*, 3–4.
13. Zhu, H.; Guo, J.; Jia, J. Correlation of the aging characteristics and deformation behavior of A357 alloy. *J. Mater. Eng. Perform.* **2001**, *10*, 186–191. [[CrossRef](#)]
14. Ragab, K.A.; Bouazara, M.; Chen, X.G. Influence of Thermal Aging Parameters on the Characteristics of Aluminum Semi-Solid Alloys. *Metals* **2018**, *8*, 746. [[CrossRef](#)]
15. Ragab, K.A.; Bouazara, M.; Chen, X.G. Quality index charts of Al-Si-Mg semi solid alloys subjected to multiple temperatures aging treatments and different quenching media. *Materials* **2019**, *12*, 1834. [[CrossRef](#)] [[PubMed](#)]
16. Avalue, M.; Belingardi, G.; Cavatorta, M.P.; Doglione, R. Casting defects and fatigue strength of a die cast aluminium alloy: A comparison between standard specimens and production components. *Int. J. Fatigue* **2002**, *24*, 1–9. [[CrossRef](#)]
17. Gan, Y.X.; Overfelt, R.A. Fatigue property of semi-solid A357 aluminum alloy under different heat treatment conditions. *J. Mater. Sci.* **2006**, *4*, 7537–7544. [[CrossRef](#)]
18. Hegazy, S.; Rahnejat, H.; Hussain, K. Multi-body dynamics in full-vehicle handling analysis. *Proc. Inst. Mech. Eng. Part K J. Multi-Body Dyn.* **2000**, *213*, 19–31. [[CrossRef](#)]
19. Ning, X.; Zhao, C.; Shen, J. Dynamic analysis of car suspension using ADAMS/Car for development of a software interface for optimization. *Procedia Eng.* **2011**, *16*, 333–341. [[CrossRef](#)]
20. Viqaruddin, M.; Ramana Reddy, D. Structural optimization of control arm for weight reduction and improved performance. *Mater. Today Proc.* **2017**, *4*, 9230–9236. [[CrossRef](#)]
21. Ragab, K.A.; Bouaicha, A.; Bouazara, M. Optimization of Casting Design Parameters on Fabrication of Reliable Semi-Solid Aluminum Suspension Control Arm. *J. Mater. Eng. Perform.* **2017**, *26*, 4450–4461. [[CrossRef](#)]

22. Nadot, Y.; Denier, V. Fatigue failure of suspension arm: Experimental analysis and multiaxial criterion. *Eng. Fail. Anal.* **2004**, *11*, 485–499. [[CrossRef](#)]
23. Wang, Q.G.; Apelian, D.; Lados, D.A. Fatigue behavior of A356/357 aluminum cast alloys: Part II—Effect of microstructural constituents. *J. Light Met.* **2001**, *1*, 85–97. [[CrossRef](#)]



© 2020 by the authors. Licensee MDPI, Basel, Switzerland. This article is an open access article distributed under the terms and conditions of the Creative Commons Attribution (CC BY) license (<http://creativecommons.org/licenses/by/4.0/>).